Predicting the Representative Elementary Volume by determining the evolution law of the convergence cone

Zwarts, Sijmen; Lesueur, Martin

DOI
10.1016/j.gete.2024.100594

Publication date
2024

Document Version
Final published version

Published in
Geomechanics for Energy and the Environment

Geomechanics for Energy and the Environment 40 (2024) 100594

Contents lists available at ScienceDirect

Geomechanics for Energy and the Environment

journal homepage: www.elsevier.com/locate/gete

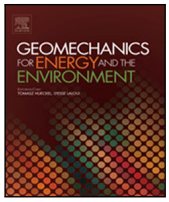

Predicting the Representative Elementary Volume by determining the evolution law of the convergence cone

Sijmen Zwarts *, Martin Lesueur

Civil Engineering and Geosciences, Delft University of Technology, Delft, Netherlands

ARTICLE INFO

Editors-in-Chief:
Professor Lyesse Laloui and Professor Tomasz Hueckel

Keywords:
Representative elementary volume
Statistics
Permeability
Digital rock physics

ABSTRACT

In order to characterise a rock formation prior to subsurface operations, it is required to find a microscale rock volume for which the homogenised property does not fluctuate when the size of the sample is increased; the Representative Elementary Volume (REV). Its determination usually comes at the cost of a large number of simulations, making it overall a computationally expensive process. Therefore, many scientific studies have been dedicated to optimising the process of finding REV. Using statistical numerical methods, it is shown that the fluctuation of the effective property corresponds overall to a cone-like shape convergence. We suggest determining the generic evolution law of the cone of convergence, which can be used to predict the size of the REV and the effective physical property. This study is based on simulations of Stokes flow through idealised microstructures from which the permeability is upscaled. By tracing and plotting the convergence of permeability for multiple samples, the full cone of convergence appears. The cone shows exponential growth and decay, converging towards the effective permeability of the microstructure. By fitting a log-normal distribution on the collected data points, we show that the generic evolution law of the cone of convergence can always be described with two parameters, independently of the porosity. We show that the determined law of the cone also applies to real microstructures, despite the presence of natural heterogeneities. The new method allows us to reduce the computational costs of finding all characteristics related to REV by simulating several subsamples rather than the full-sized sample, unlocking thereby high-resolution samples which are often too computationally expensive. The use of a statistical model provides quantification of the precision level we can obtain on the REV determination.

1. Introduction

Rock mass characterisation remains an important task in geoscience since underground formations are still being considered for subsurface operations of sustainable interest, such as geothermal production or CO2/H2 storage. To understand the behaviour of rocks and their properties, it is essential to study the microscopic scale. For example, porosity, connectivity of the voids and other morphologic parameters directly influence the rock's permeability.[1–3] However, modelling larger systems from their microstructures is not practical, as it requires excessive computational power to capture the microscopic complexity. Digital Rock Physics (DRP) provides a scheme to upscale the physical properties of the heterogeneous porous media to the macroscopic scale.

The upscaling of the physical properties from the microstructure to the macroscale requires the determination of the Representative Elementary Volume (REV). This is the smallest volume of a heterogeneous sample that can accurately represent the mean constitutive response at the macroscale. In DRP, defining the REV is crucial since the physical properties of the porous media vary significantly at the microscale. This makes it difficult to model and predict the behaviour of the rock on an upper scale based on microscopic samples. By identifying and characterising the REV, the physical quantities can be upscaled from the microstructure and used for macroscale applications. Another benefit of REVs is the ability to apply multiscale modelling. The homogenised macroscopic response is used as input to the microscopic boundary value problem, which in turn provides the material response at the macroscale. This circular system allows for the determination of non-linear physical responses in the overall material behaviour without making too many approximations.

While the REV determination is a fundamental exercise in DRP, it remains a challenging task due to the complex nature of the porous media considered. To find the physical effective properties of the microscopic samples, homogenisation is applied to a growing subsample. Smaller volumes of the porous medium can exhibit significant variances in the properties, thus simulations on larger volumes are needed to

* Corresponding author.
E-mail address: s.zwarts@tudelft.nl (S. Zwarts).

https://doi.org/10.1016/j.gete.2024.100594
Received 22 April 2024; Received in revised form 3 September 2024; Accepted 6 September 2024
Available online 10 September 2024

achieve convergence towards a stable value. Tracing this convergence is computationally expensive, especially when dealing with large volumes that are extremely computationally demanding in both resources and time. On top of that, the resolution of CT-scan imaging continues to increase (e.g. 0.7 μm reported by Ref. 4) leading to even more expensive simulations.

Therefore, researchers have tried to simplify and optimise the process of finding REV. Some studies have shown that the REV can be related to the grain size or other morphological parameters, for selected physical properties. Ref. 5 showed that the number of grains required for homogeneous elastic behaviour of polycrystalline should be at least 230. Ref. 6 tested over 500 cubic polycrystals in the plane stress problem and showed that the REV size of the polycrystals is roughly 16 times the grain size. Ref. 7 determined experimentally that the minimum size to represent uniaxial compression and thermal expansion of PBS 9501 heterogeneous materials with an average crystal diameter of around 100 μm is approximately 1.5 mm. Ref. 8 studied bone biomechanical behaviour and showed that the REV size of the elastic coefficients of the tissue is about 1.5 mm. There are many more examples of studies for different physical properties of different materials, that define REV at a specific size. However, if the input parameters – such as the type of material or physical property being assessed – are changed, the size of the REV will change unpredictably.

Instead, generic methods have also been developed to find REV which do not necessarily depend on a specific property or type of material. Ref. 9 introduced a methodology involving the use of stereological and image analysis techniques to quantitatively characterise the microstructure of ceramic matrix composites. This is used to create a computer-generated REV which is statistically representative of the real microstructure, including fibre-rich and -poor regions. Ref. 10 suggested a representative unit cell approach, assuming a unit cell to be periodic over a specific sample to find the REV, which is characterised by a power law particle size distribution. Yet, while these methodologies provide useful approaches for finding the REV in different materials and media, they are still time-consuming and require significant computational power.

To get more insight into the evolution of the REV convergence, numerical–statistical methods have been applied in the process of finding REV. Ref. 11 studied the geometrical properties of the microstructure and showed that the variance of the particle distribution within the sample converges with an increasing measured area. Ref. 12 presented the rate of convergence based on the number of grains in the length of a cubic sample, depending on the porosity, with a decreasing variance of the porosity considering larger samples. Ref. 13 studied the heat flow and the linear elasticity of a random medium. They applied a two-point probability and a lineal-path function to find a converged value of the physical properties. Ref. 14 computed the REV for linear elastic properties and thermal conductivity including a convergence of the variance considering larger samples. They showed that the properties can be determined not only using numerical simulations on large volumes but also with mean values of multiple small volumes. Ref. 15 continued the work using a new stopping criterion to reduce computational costs, which is especially convenient in non-linear cases. Ref. 16 used the statistical–numerical approach to find the REV for polymers subjected to finite deformations with a predefined percentage of the average deformation and a predefined error as the stopping criteria. Ref. 17 homogenised a REV for composites to find the elastoplastic response for transverse tension and longitudinal shear and shows the convergence towards a certain stress level with a decrease in scatter. Similar types of graphs, displaying the REV convergence for the directional moisture diffusion within glass/epoxy composites, are shown by Ref. 18. Ref. 19 showed the REV convergence for porosity for five different rock samples and demonstrated that the variance of the porosity can be used as a qualitative indicator for rock heterogeneity. Ref. 20 looked for the mean and bounds of the REV convergence of a dataset of multiple rock samples to prove the convergence of the permeability tensor asymmetry to zero at REV and clearly shows that the process of finding the REV results in a cone-shaped convergence pattern of the physical property.

The numerical statistical studies all demonstrate that the property varies substantially when different smaller volumes are considered and as the size of the samples is growing, the variance of the property will decrease and converge towards a stable value. When the variance of the property is small and the average value of the property has stabilised, the size of the REV can be determined. Due to the direct correlation between the geometric properties of the microstructure and the homogenised physical quantity, the convergence is always bounded by the cone shape, starting with a wide base and becoming increasingly narrow with a growing sample size.

In this study, we propose a new method to find REV, by making use of the known shape of the cone of convergence. The shape provides information on both the rate of convergence and the value of the homogenised property, allowing us to find the REV in a more accurate way. In addition, if the digital rock sample is not large enough to find REV, which is often the case considering carbonate rock samples for example, the cone of convergence can still provide information about the expected size of the REV and homogenised property value. With a focus on permeability, a property of significant interest in DRP, we aim to find the evolution law of the REV convergence cone. The energy dissipation will also be considered due to its relevance to homogenisation schemes.[21]

This paper is organised as follows. In Section 2, we do a benchmark study with idealised microstructures and determine the generic evolution law of the REV convergence cone. In Section 3, the law is applied to real microstructures, to validate whether the generic evolution law still holds when natural heterogeneities interfere. In Section 4, the requirements to apply the method are discussed and compared to traditional methods.

2. Material and methods

For the benchmark study, we consider an ideal porous medium, random packing of perfectly round spheres. As such, by avoiding the influence of the grain properties, we aim in this section to find the generic evolution law of the REV cone of convergence. In this contribution, we follow the research design presented in Ref. 21, which shows the set-up to generate the random packings, the mesh, the Stokes-flow model and the postprocessing of the permeability and energy dissipation of the fluid transport.

With Finite Element simulations of Stokes-flow run in MOOSE,[22,23] we can calculate the energy of the fluid transport and the permeability of the samples. With the recommendations of Ref. 24 in mind, the postprocessing of the effective properties are applied within a subvolume away from the boundary layer, without the influence of the boundary conditions. We follow the recommendations from Ref. 21 and plot the evolution of the energy consistency index with increasing subsample size to determine the REV of the permeability. The index is defined as the ratio between the macro- and micro-scale energy. At REV, we respect the Hill–Mandel principle and obtain therefore the energy consistency across scales, which means that the index becomes unitary.

2.1. Generating the cone of convergence

The REV convergence cone represents the convergence of homogenised properties for samples with increasing size. The cone consists of a collection of data points, each representing the value of a homogenised property obtained from different samples that vary in size and morphological properties of the microstructure. At small sizes, close to the scale of the local heterogeneities of the porous medium, we obtain a substantial variability of the homogenised properties. Larger sizes, including more grains, are more representative and approach

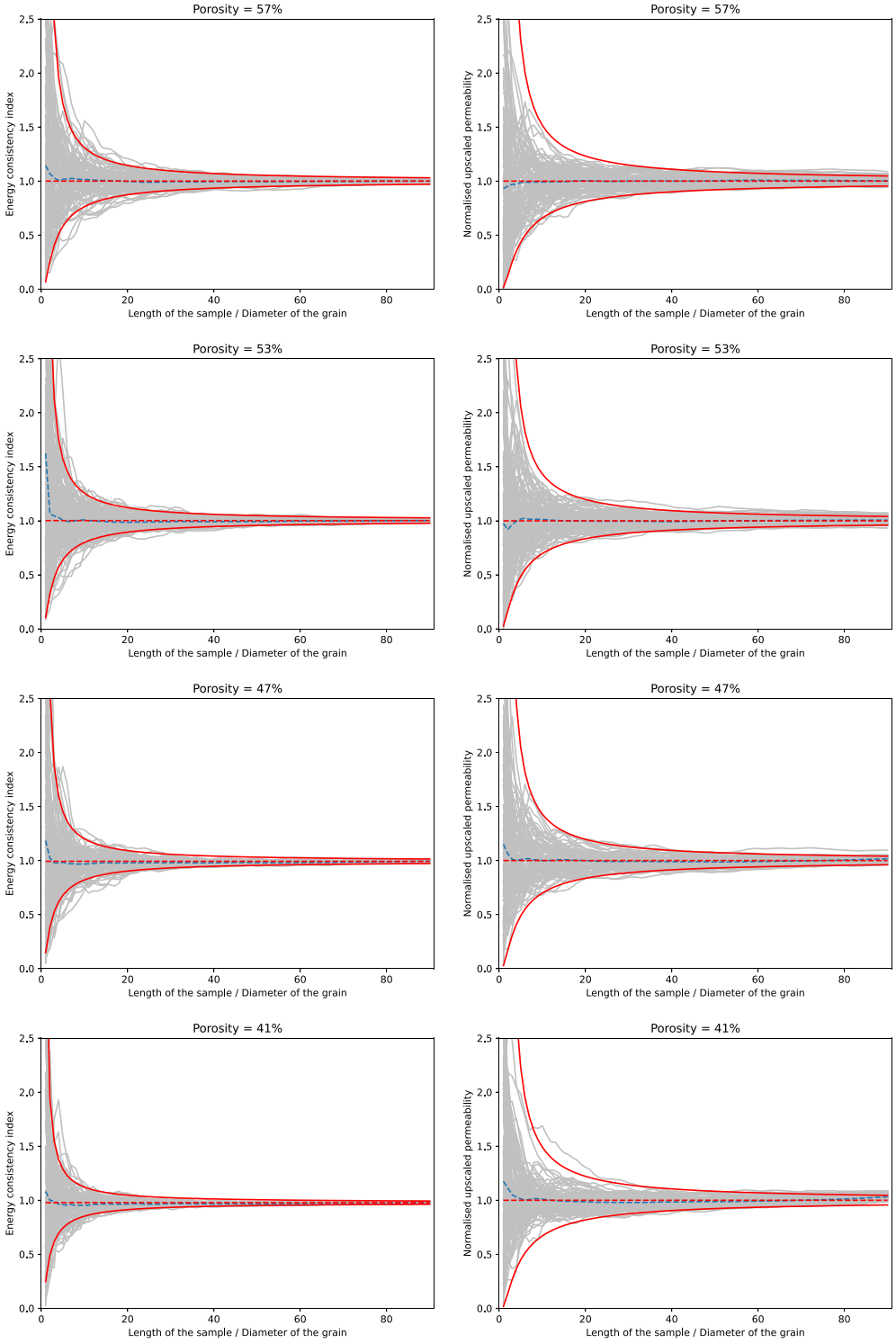

Fig. 1. The different REV convergence cones of the random packings of different porosities. The left column displays the evolution of the energy consistency index of various porosities and the right side shows the normalised permeability. The grey lines show the evolution of the individual random packings and the blue dashed line the mean value of the property. The red lines are the determined evolution law of the cone, with the mean value plotted in a dashed line and the boundaries as continuous lines.

REV, which means that the homogenised property converges towards a specific value. As such, the REV convergence follows a cone shape.

In this research, the data points are obtained by tracing the evolution of energy dissipation and permeability for a series of random packings with the same characteristics. For each sample, the properties are traced on a subsample growing in size starting from the centre of the random packing, gradually to the maximum size of the sample. This method of tracing the REV convergence, validated by Ref. 21 allows to reduce the number of simulations needed to one – for the full sample – and the data points are obtained with postprocessing. We repeat the

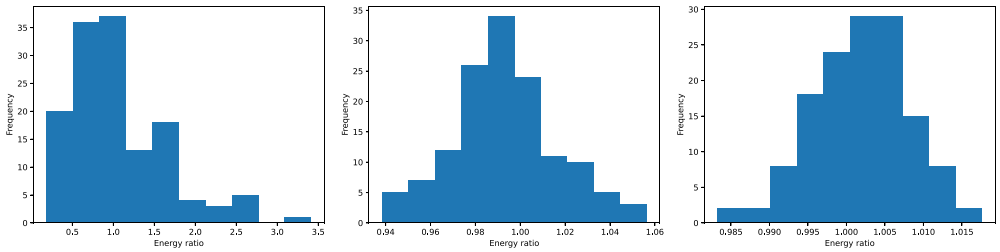

Fig. 2. Histograms of the energy consistency index at a minimum, half and maximum subsample size of the samples with a porosity of 53%.

process for a series of samples and plot it all together in the same graph, see Fig. 1. To obtain statistical representativeness, we consider 100 samples for each porosity, which ranges from 33% up to 74%. At a first glance, this number of models already allows to visually display the cone of convergence.

2.2. Evolution law of the REV convergence cone

The overall shape of the REV convergence cone is visualised through the superposition of the trace of the individual samples, shown with grey lines in Fig. 1. Note that the missing spaces present in the cone would be filled if more statistical representativeness is considered. All the cones start with a wide base and converge towards a specific value, as shown by the decreasing width of the cone. The mean value of the homogenised property, considering all individual samples, is plotted with a dashed blue line. Compared to the overall convergence of the cone, we observe a faster convergence of the mean value. Once the mean value has stabilised, its value is the true effective homogenised property. As mentioned previously, we confirm that the energy consistency index mean value is always one.

Based on the distribution of the data points at each size s and since the energy dissipation and the permeability are inherent average properties of the rock sample, the boundary of the cone y can be, from a statistical point of view, described with a mean value μ and a standard deviation of the mean σ:

$$y_s = \mu_s \pm \sigma \tag{1}$$

In probability theory, the central limit theorem states that a distribution converges towards a Gaussian distribution when considering large and independent datasets. However, we observe that the overall shape of the cone exhibits asymmetry around the mean value, in contrast to the perfectly symmetric Gaussian distribution. A closer examination of the histogram of the samples with 1% size of the full sample, shown in Fig. 2, presents values between zero and over 2.5 for the energy consistency index while the mean value remains unitary. This range of values is realistic since at the scale of a single grain size the flow can either be fully obstructed by the rock grains (resulting in zero permeability) or have a completely unobstructed flow path (leading to high values). The same holds true for the energy consistency index. This aspect has for consequence that the cone is not exactly symmetric around the mean value for samples at the size of one or a few grains. Interestingly, when more grains are included in the sample, symmetry is recovered and a smaller range of values between 0.94 and 1.05 is centred around the energy consistency index of one, which corresponds to a more representative flow path on the macroscale. Due to the asymmetric shape of the distributions, we apply a modified version of the central limit theorem, commonly known as Gibrat's law, and fit a log-normal distribution to our data. The log-normal distribution exhibits an asymmetrical range between zero and infinity, which therefore includes the very high values observed at the beginning of the cone but excludes values below zero. We note that as the variance, which is the squared value of the standard deviation, of a log-normal distribution decreases, the difference with a normal distribution becomes negligible, which creates a more symmetric shape as observed in our case with volumes approaching the full sample size. For simplicity, we will subsequently refer to the log-normal standard deviation of the distribution $\sigma_{ln;s}$ for a certain size with σ_s:

$$\ln y_s = \ln \mu_s \pm \sigma_s \tag{2}$$

Focusing on the mean value, we observe its convergence within the first segment of the cone to a stabilised value, for each cone in Fig. 1. The fluctuation observed with samples containing only a few grains can be attributed to the wide range of the values, leading to an increase in the standard error of the sample,[25] and thus the mean can be considered stable over the whole evolution of the convergence. Considering the total number n_{tot} of data points x, we approximate the mean value of the log-normal distribution μ with the weighted geometric mean $\langle \ln x \rangle$, proportional to the sample volume V_i.

$$\mu \approx \langle x \rangle = \exp \frac{\sum_i^{n_{tot}} \ln x_i \cdot V_i}{\sum_i^n V_i} \tag{3}$$

For the determination of the variance, we make use of the law of large numbers, which describes that the variance of a mean from a number of independent observations of the same distribution is calculated by taking the average of the variance of the sum. We note that in our case, as the sample size increases, smaller samples are encompassed within the larger sample sizes. Considering that permeability is a mean homogenised property, we can assume that the permeability of a sample is equal to the average permeability for a certain number of subsamples, which together are equal in volume to the sample of interest. This principle is schematically shown in Fig. 3.

To apply this principle, we introduce a reference sample V_{ref} and establish a relationship with a sample with a specific size V_s by considering the number of reference subsamples n_{ref} that can fit within the volume of the sample of interest. This relationship is expressed as:

$$\sigma_s^2 = Var\left(\frac{\sum_{i=1}^{n_{ref}} x_i}{n_{ref}}\right) = \frac{\sum_{i=1}^{n_{ref}} Var\left(x_i\right)}{n_{ref}^2} = \frac{1}{n_{ref}^2}\left[n_{ref}\sigma_{ref}^2\right] = \frac{\sigma_{ref}^2}{n_{ref}} = \frac{V_{ref}}{V_s}\sigma_{ref}^2 \tag{4}$$

Note that the number of samples is equal to the volume ratio of the reference subsample size to the size of interest. To ensure that the observations are independent, we suggest considering only the largest samples as the reference samples, as including smaller subsamples would make the observations of the effective properties dependent on each other since the larger samples include the data of the smaller samples. The variance of the log-normal distribution for an arbitrary size s can now be described as a relationship to a constant reference value, which is calculated as per the definition of variance:

$$\sigma_s^2 = \frac{V_{ref}}{V_s}\sum_{i=1}^{n_{ref}}\left(\ln\frac{x_i}{\mu}\right)^2 \tag{5}$$

To assess the validity of coupling the variance for a specific size with the reference variance and the size ratio, we compare the formula with the variance calculated individually for each size, in Fig. 4. We obtain approximately the same values with both methods and can therefore conclude that the mean values of the reference subsamples are indeed

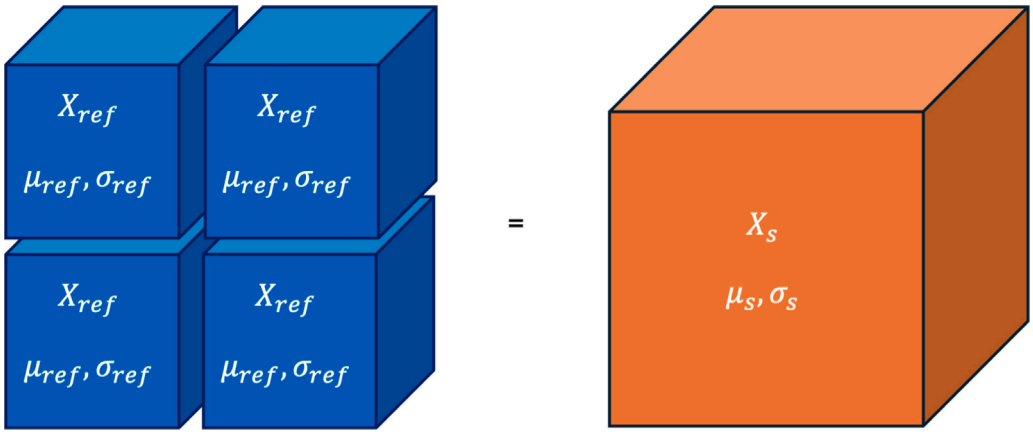

Fig. 3. An abstract visualisation of the correlation of the physical properties X, the mean value μ, and the variance σ of the reference subsamples and a specific sample of interest, in which the sample of interest encompasses the reference subsamples.

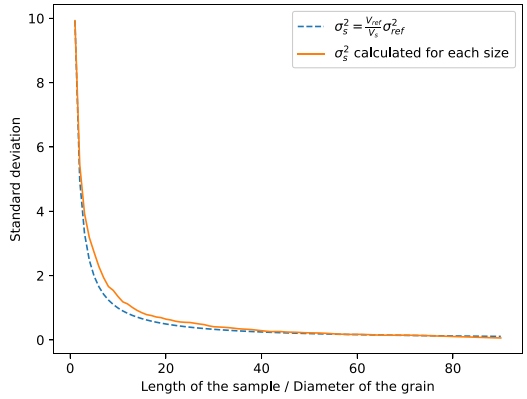

Fig. 4. Evolution of the standard deviation according to the size of the model. The orange line is the standard deviation computed per sample size and the blue dashed line is the standard deviation as a function of the sample size and our reference value, computed on the largest size considered.

correlated to the mean of samples with a specific size and consequently can be used to describe the evolution of the variance. Note that this relation still holds, even if the size of the reference sample is larger than the size of the sample of interest.

With both the mean value and the variance described, the boundary of the cone, shown in Eq. (2), can now be rewritten in terms of the mean value, a reference variance and a size ratio:

$$\ln y = \ln \mu \pm \sqrt{\frac{V_{ref}}{V_s}}\sigma_{ref} \quad \Leftrightarrow \quad y = \mu \cdot \exp\left(\pm\sqrt{\frac{V_{ref}}{V_s}}\sigma_{ref}\right) \tag{6}$$

The width of the base of the cone is also associated with the number of standard deviations considered, as determined by the Empirical Rule. Considering the statistical presence of potential outliers in the observations, which can impact the boundaries of the cone, we incorporate twice the standard deviation in our fitting approach, which includes 95% of the data.

$$y = \mu \cdot \exp\left(\pm 2\sqrt{\frac{V_{ref}}{V_s}}\sigma_{ref}\right) \tag{7}$$

In the two-dimensional case, which applies to the random packings, the volume is equal to the square of the length $V_s = L_s^2$. As the permeability and REV convergence are typically plotted with respect to the sample length, the evolution of the cone of the REV convergence is described as

$$y = \mu \cdot \exp\left(\pm 2\frac{L_{ref}}{L_s}\sigma_{ref}\right) \tag{8}$$

In the three-dimensional case, which typically applies when analysing real samples, the evolution of the cone is described as

$$y = \mu \cdot \exp\left(\pm 2\left(\frac{L_{ref}}{L_s}\right)^{3/2}\sigma_{ref}\right) \tag{9}$$

2.3. Fit of the determined evolution law

From the data points of Fig. 1, for both the energy consistency index and permeability, we calculate the mean value and the variance of the reference size taken as the largest and using Eq. (8), we plot the evolution of the fitted log-normal distributions in Fig. 1. The boundaries of the distribution, determined by the variance, are shown with a red line and the mean value with a red dashed line. We observe that the mean value determined with the log-normal distribution accurately describes the stable average value of properties of the samples, as they superpose in the figure. The boundaries of the log-normal distribution also visibly correspond with the boundaries of the REV convergence cone. This confirms that fitting a log-normal distribution on the data points is adequate to describe the shape of the cone and can therefore be used to describe the convergence behaviour. The cone appears to always follow the same shape and only differ by the value of convergence and its rate, reflected in the fitting parameters.

The fit of the REV convergence cones of the energy consistency index appears to exclude more outliers than the cones of the permeability, despite having similar proportions of data points fitting within the mathematical model with twice the standard deviation. The outliers of the convergence cone of the energy consistency index are particularly visible as they appear near the start of the cone. While the overall shape and evolution law of the REV convergence cones remain consistent, we observe that the convergence behaviour is dependent on the porosity of the sample, since some porosities result in wider base widths of the cones compared to other porosities. For instance, the width of the energy consistency index convergence cone with a porosity of 53% is nearly double the width of the cone with a porosity of 41%. The correlation between the reference variance and the porosity is presented in Fig. 5. In the figure, the standard deviation shows distinct values for each porosity. For both the permeability and energy consistency index convergence, we observe that at lower porosities the value of the standard deviation decreases, until a porosity of 35%. For the energy consistency index, the standard deviation increases past this point, following a linear trend, reaching 2.25 at 76% porosity. The differences

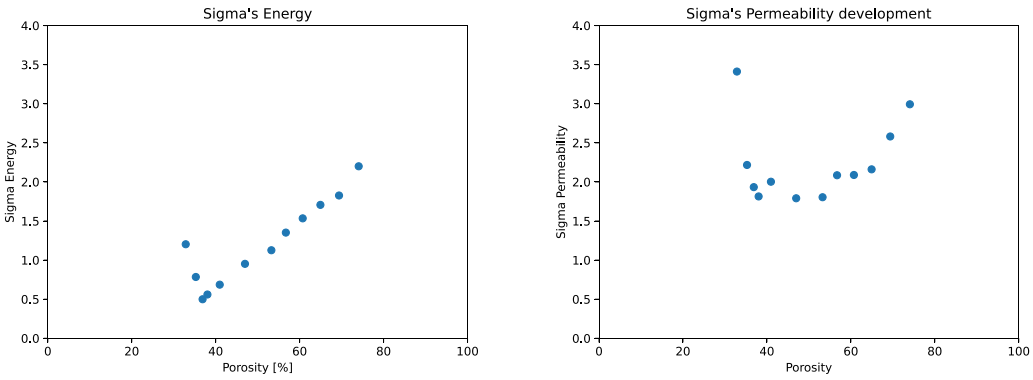

Fig. 5. The evolution of the standard deviation compared to the porosities of the random packings. On the left the standard deviation of the energy consistency index is shown, and of the permeability on the right.

in the standard deviation values indicate that even though the heterogeneities of the grains are excluded in the random packings, other morphological properties of the microstructure, such as the porosity here, still influence the convergence of effective properties. Specifically, the chaotic correlation, observed with the permeability, suggests that more morphological parameters influence the convergence. The less chaotic and clearly linear trend from the energy consistency index in comparison to the permeability confirms the observations of Ref. 21, that the new index that was introduced in that study is a better indicator of permeability REV.

Having confirmed the adequate fit of the log-normal distribution, we can leverage the additional properties of this statistical model. While the description of the convergence towards the effective property with the statistical model offers insights into the accuracy of the REV size, the statistical model also allows us to quantify the error made on the fit of the cone itself, considering both the mean value and the standard deviation.[26] As the standard deviation determines the width of the cone, its error directly impacts the width of the cone and consequently the convergence behaviour. We can relate the error ϵ directly to the reference standard deviation with

$$\frac{\epsilon}{\sigma_{ref}} = \frac{1}{\sqrt{2n_{ref} - 2}} \tag{10}$$

We present the convergence of the reference standard deviation with the number of samples considered in Fig. 6 for three different porosities, considering the REV convergence of the permeability. The continuous line in the plot presents a convergence of the standard deviation towards a specific value as the fluctuation dampens out with an increase of the number of samples. We also plot the boundaries of the estimated error with the dashed lines, calculated by multiplying the relative error shown in Eq. (10) with the corresponding standard deviation. Since the value of the standard deviation is not completely stabilised yet, we take the value of the standard deviation with the maximum number of samples (100), as this provides the best estimate of the converged value (still a calculated error of 7%). We observe that the evolution of standard deviation with the number of samples is accurately described with the use of the equation and can therefore be used to determine the size of the models when a specific accuracy of the fit of the cone is required.

The value of the standard deviation decreases when larger samples are considered, as shown by the cone of convergence. However, we note that the relative error solely depends on the number of samples considered and not on the value of the standard deviation itself. This implies that the relative error when considering different sample sizes is the same for each size. Therefore, any subsample size can be selected in order to fit the REV convergence cone. Consequently, this means that simulations on large samples are not required since theoretically, the simulations on smaller samples would estimate the REV convergence cone with the same level of accuracy.

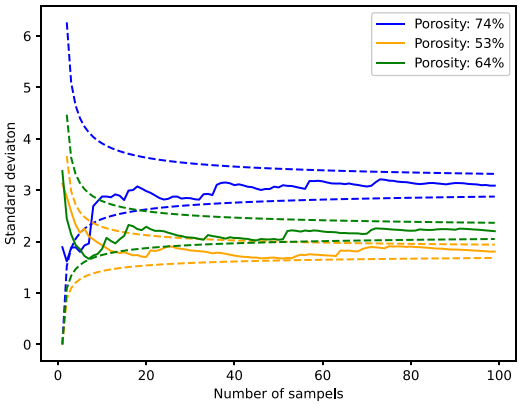

Fig. 6. Three examples of the evolution of the reference standard deviation of the permeability with respect to the number of samples considered. The solid line is the evolution of the standard deviation and the dashed line shows the boundaries of absolute error.

3. Application to real microstructures

The previous section confirms the existence of the REV convergence cone and shows that the generic evolution law of the convergence can be described by fitting the data points in a log-normal distribution. Our benchmark was done on idealised microstructures, and we aim now to verify if the law we derived in Section 2.2 also applies to real rock microstructures. These contain natural heterogeneities which may affect the evolution of the cone of convergence and disturb our fit. This section will analyse samples of increasing heterogeneity.

The reconstruction of digital rocks follows the methodology proposed by Ref. 27. To start with, a stack of 2D μCT-scans grey-scale images are subjected to segmentation and subsequently transformed into 3D computational models, enabling the differentiation between rock and void spaces. To optimise computational efficiency during simulations, the Displaced Boundary method, introduced by Ref. 28, is used. This technique enables the pore-boundary interface to be conformed to a coarser background mesh, leading to reduced mesh file sizes at mesh convergence. The larger simulations on the real rock samples are run on the DelftBlue supercomputer.[29]

Contrary to random packings, rock samples provide limited data due to the natural limits of physical sample size and scan resolution. As we require the input of several independent samples to fit our law with more accuracy, the full rock sample is split into multiple subsamples. To enforce that the subsamples still reflect the permeable behaviour of the rock, the subsamples cannot be excessively small, as they may not have reached the percolation threshold yet. Larger samples lead to a better representation of the flow behaviour through the rock, yet

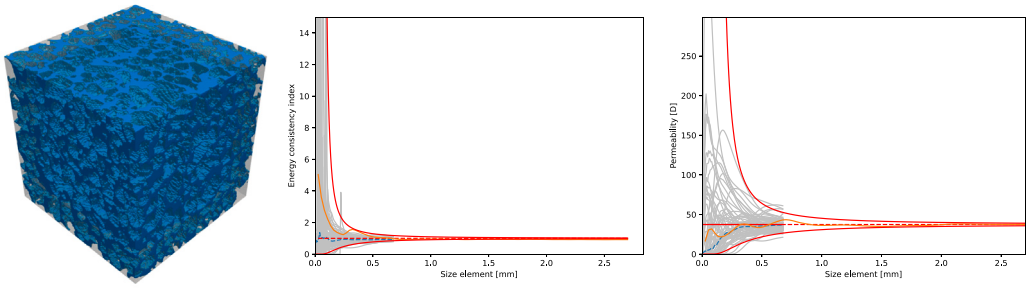

Fig. 7. The results for the LV60A sandpack. On the left, the pore space of the sandpack is shown. The middle graph shows the REV convergence cone of the energy consistency index and the right graph shows the permeability, with our fitted law shown with a red colour.

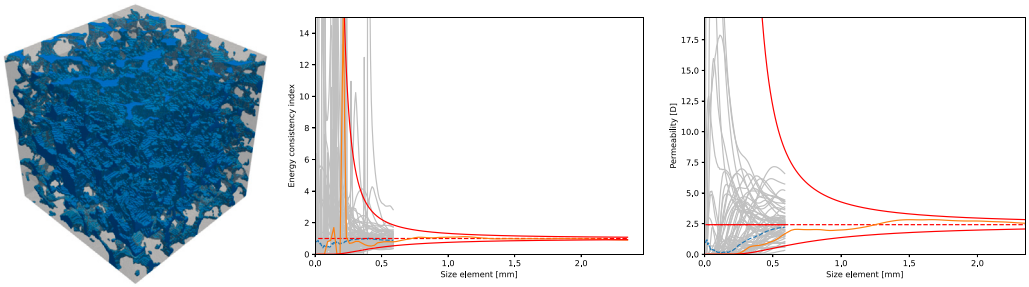

Fig. 8. The results for the S1 sandstone. On the left, the pore space of the sandstone is shown. The middle graph shows the REV convergence cone of the energy consistency index and the right graph shows the permeability, with our fitted law shown with a red colour.

their lower number comes at the cost of a higher error, according to Eq. (10). As a compromise, each rock sample is cut into four equal parts in three dimensions, resulting in 64 subsamples which gives a relative fitting error of 9%. To maintain the independence of the postprocessed permeability and energy dissipation within each subsample, there is no overlap between the samples.

3.1. LV60A sandpack

The first rock sample in this study is the LV60A sandpack,[30] which is displayed in Fig. 7a. While the sand pack is relatively homogeneous for a real rock sample, it still contains natural heterogeneities in the grain properties, such as grain roughness and non-sphericity. The sandpack has high permeability owing to the good connectivity of its voids, shown with a porosity of 38% and a characteristic length of 149 μm. Note that we compute the characteristic length as introduced by Ref. 31. These properties make it a good starting point for verifying the identified evolution law of the REV convergence cone. The LV60A sand pack sample has a size of just over three mm and is scanned using a resolution of 10.008 μm, resulting in 300^3 voxels. The cones of convergence for both the permeability and energy consistency index of the sandpack are shown in Fig. 7b and c.

The REV convergence cone of the sandpack presents a difference in magnitude compared to the random packings as we observe on the sand pack a wider base of the cone with values going over 14 for the energy consistency index and 300 D for the permeability, does not affect the fitting of the cone of convergence. Still, both the energy consistency index and the permeability present a good fit of the law determined from the random packing. We also observe that the lack of percolation within small subsamples, shown with an energy consistency index and permeability of zero (up to a size of 0.25 mm), is also included in the fit. This highlights the adequacy of the asymmetrical nature of the log-normal distribution. We also observe that the converged values at the full sample size of both properties are within the cone of convergence, from which we conclude that the determined evolution law is accurate in predicting the homogenised properties. Visually, it appears that the convergence of the energy index is fitted more accurately, compared to the convergence of the permeability, due to the presence of empty spaces observed in the permeability data. However, this can be attributed to the fact that the variance of the permeability cone is much larger than the variance of the energy consistency index. We know, from the log-normal distribution, that the likelihood of obtaining observations on the edges of the distribution is lower, specifically on the higher range of values. Consequently, the lower part of the cone appears to be better fitted than the upper part. We use the evolution law of the REV convergence cone to determine the permeability and the size of the REV and obtain values that align with those reported by Ref. 32. The permeability is found to be 37 Darcy, which is within a five per cent margin of 39 Darcy noted by that study. They found REV at a length of 1.1 mm for the permeability, at which we measure a margin of only four per cent using the REV convergence cone of the energy consistency index.

3.2. S1 sandstone

The second sample in this study is the S1 sandstone,[33] shown in Fig. 8a. Unlike sandpacks, which consist of individual grains, sandstone is a type of rock with a cohesive structure in which the grains are cemented together by minerals. Sandstones tend to have lower permeability due to the lower connectivity of their voids and the more tortuous flow paths. As a result, the S1 Sandstone exhibits slightly more heterogeneous properties, shown with a porosity of 20% and a characteristic length of 311 μm, which makes it harder to find REV. The S1 sandstone is scanned with a resolution of 8.7 μm over a total length of just over 2.6 mm, resulting in 300^3 voxels. The REV convergence cones for both the permeability and energy consistency index of the sandstone are shown in Fig. 8b and c. The results show that the lower connectivity of the voids in the sandstone, compared to the sandpack, leads to slower convergence towards the effective permeability of the rock or unitary energy consistency index, as some of the subsamples lack percolation up to a sample size of 0.25 mm or have a high energy consistency index and permeability. However, the fit with the determined evolution law does include these values, as the lower boundary of the cone can be distinguished from zero values from that size. The upper boundary of

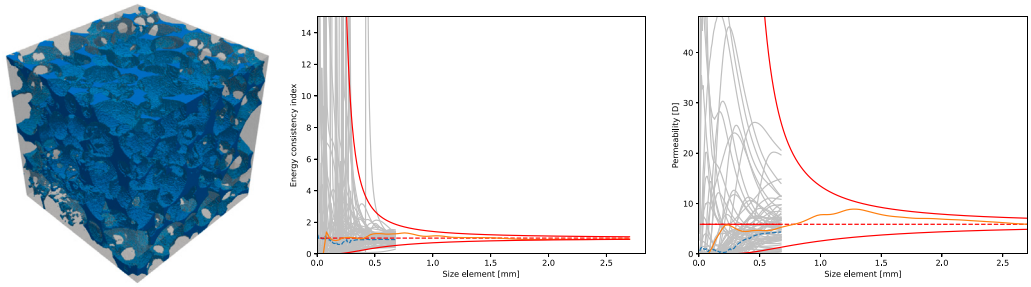

Fig. 9. The results for the Ketton limestone. On the left, the pore space of the limestone is shown. The middle graph shows the REV convergence cone of the energy consistency index and the right graph shows the permeability, with our fitted law shown with a red colour.

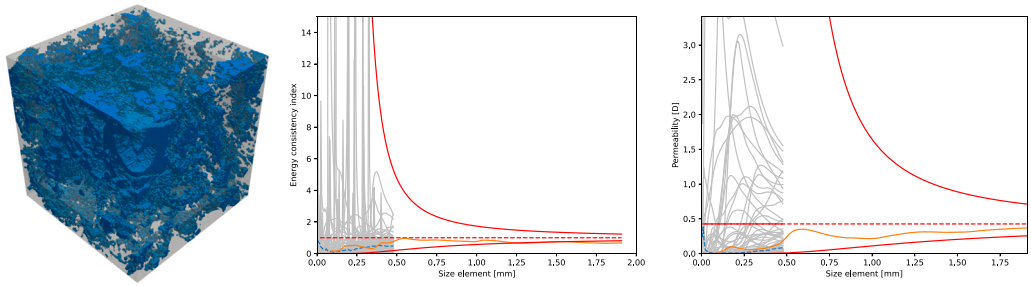

Fig. 10. The results for the carbonate C2. On the left, the pore space of the carbonate is shown. The middle graph shows the REV convergence cone of the energy consistency index and the right graph the permeability, with our fitted law shown with a red colour.

the cone does include the higher values as well, excluding a peak value around 0.5 mm, which is an outlier according to the statistical model. Above a size of 0.25 mm, it is clearly observed that the properties of the subsamples converge exponentially towards a certain value. We also observe similar trends as with the sandstone. as the energy consistency visually represents the cone better than the permeability, and the lower part of the cone is better represented. Ref. 32 has shown the REV to be around 1.3 mm in length size, yet there is still some evolution in the permeability which we also observe as the variance near the full size of the sample has a value of 0.11, almost three times as big as the sandpack. If we fit the evolution law of the cone of convergence, we find that at 1.3 mm the margin of the size of the permeability REV is around 12%.

3.3. Ketton limestone

The third sample in this study is the Ketton limestone,[34] which is shown in Fig. 9a. Limestone is typically composed of calcium carbonate and is therefore often quite heterogeneous, with substantial variance in grain shapes and sizes and non-uniformly connected pore spaces. However, this particular limestone sample is relatively homogeneous and has reasonably well-connected voids, shown with a porosity of 13% and a characteristic length of 331 μm. The sample has a high-resolution CT-scan image of three μm and with a total size of just over 3 mm, the digital reconstruction results in 1000^3 voxels. The REV convergence cones for both the permeability and energy consistency index of the limestone are shown in Fig. 9b and c. We find many similarities to the results of the S1 sandstone in both values as in trend. The fit for both the permeability and the energy consistency index is excellent and the values of the full-sized sample remain within the boundaries of the cone. Assuming REV convergence below an error of 5%, the REV would be found at approximately 1.7 mm, as determined by the energy consistency index REV convergence cone.

3.4. C2 carbonate

The final sample in this study is the C2 carbonate,[35] as shown in Fig. 10a. This carbonate exhibits high heterogeneity in grain properties and low connectivity of voids, shown with a porosity of 14% and a characteristic length of 220 μm, resulting in low permeability overall. The sample has an image resolution of 5.7 μm and a total size of just under 2.3 mm, which results in 400^3 voxels. The cones of convergence for the carbonate are presented in Fig. 10b and c. The C2 carbonate shows that the variance of the values for both the permeability and the energy dissipation are higher than observed with the previous samples. We observe that, despite considering the full subsample size, the percolation threshold is not always reached. Consequently, the fitted law only deviates from values near zero after the full subsample size. This also means that high values, above 15 for the energy consistency index, are also captured in this same region. At the maximum size of the subsamples, we observe some level of convergence, with the boundaries of the cone width decreasing significantly. Ref. 32 showed that the REV size cannot be determined for permeability, even when the full sample is considered. By extrapolating from our fitted REV convergence law, an estimation of the REV size is possible. We predict that the REV size, considering a variance of 5%, for the energy consistency index, which is known to converge to one, should have a length of 4.9 mm, which is more than double the full sample size. It is, however, challenging to verify the validity of the evolution law for the permeability of the C2 carbonate due to the high variance of the data points used for the fit. The main difference between this sample and the others is that the percolation threshold still has not been reached at the full subsample size, which seems to influence the accuracy of the fit.

4. Method requirements and computational performance

This section discusses the subsample requirements to fit our law in order to find REV. For users of our method, it is important to understand how to control the error made on the REV estimation. In Section 2 it was established that the relative error is theoretically solely dependent on the number of subsamples considered and independent of the magnitude of the variance. However, as demonstrated in Section 3, considering a subsample size below the percolation threshold leads to a significant increase in the variance, making it challenging to validate the evolution law effectively due to the observed empty spaces. In addition, while the relative error should not be influenced by the

subsample size, the absolute error is larger with higher variance values and therefore leads to a bigger deviation of the fitted cone from the true boundary of the REV convergence cone.

To overcome this pitfall, we recommend finding pre-emptively the percolation threshold, in order to consider a subsample size past the threshold, where the variance has drastically reduced. Additionally, choosing the smallest subsample size just above the percolation threshold has the advantage of maximising the number of samples which reduces the error of the fit and therefore provides the best estimation for the convergence of the size of the REV and its properties.

This subsampling offers the obvious benefit to reduce the amount of computational resources required to determine REV. Memory usage for each of our simulations is shown in Appendix to scale linearly with the number of degrees of freedom – as theoretically expected– and therefore fits a cubic power law with the length of a 3D sample. If we compare our method, where the memory requirement is related to the size of the subsamples of length l, to the traditional method where we need the memory to simulate the full sample of length L, then by introducing the ratio $\eta = \frac{L}{l}$, we obtain a decrease in memory use of $1/\eta^3$ with our method.

To give a few examples, we determined that the simulations run in sequential for the REV of the LV60A sandpack – found at 120 voxels length by Ref. 32 – require a minimum memory requirement of over 280 GB, corresponding to three nodes of 128 GB on the DelftBlue supercomputer we use. However, the subsamples of 83 voxels length used in the case study of Section 3 require only 92 GB, which allows to run the simulation on a single node and additionally provides more statistical information about the REV convergence. While there will be an increase in access to computational resources over the years (e.g. the DelftBlue supercomputer offers memory nodes with access to 1.5 TB of memory[29]), larger samples will exceed this memory availability rapidly due to the cubic increase of memory requirement with the sample size. In the case of the C2 carbonate, for example, we already see a large increase of the REV numerical size, to 860 voxels. On top of that challenge, recent developments in CT-imaging and the segmentation into computational models, produce microstructures with a length going up to multiple thousands of voxels.[36,37] To stay ahead of this race between computational resources requirement and accessibility, the method of the REV convergence cone provides a possibility to unlock those large and/or high-resolution samples.

A similar comparison is made for the simulation run time. As shown in Appendix, the CPU run time follows a classical power law with the length of a 3D sample, as expected from the Generalised Minimal Residual Method solver used. By using the subsample size ratio η, we obtain with our method a run time speed-up of $\eta^{3(d-1)}$, with $d > 1$ that depends on the efficiency of the solver.

As an example, we observe that an equivalent volume of the full sample of the LV60A sandpack (300 voxels) can be simulated with subsamples just above the percolation threshold (40 voxels) 2.5 times faster. On top of this, the lower memory requirement enables an efficient parallelisation of the simulations, which means that the wall time itself can be drastically decreased, depending on the computational resources available.

5. Conclusion

In conclusion, this paper presented a computationally cheap yet efficient method to find the Representative Volume Element (REV). From a statistically representative set of samples of idealised microstructures, we show that the REV convergence of an effective property – here focused on permeability and the energy consistency index introduced in Ref. 21 – follows a cone of convergence, with exponential growth and decay towards a converged value. Derived from statistical relationships, we describe the boundaries of this cone as the variance of a log-normal distribution centred around its mean value which represents the REV value. By fitting a log-normal distribution, we obtain additional information that cannot be obtained using the traditional REV convergence method, about the accuracy of our fit and of the REV size prediction.

Our method is tested on real rock samples and successfully determined the REV size of previously benchmarked samples. While the natural rock heterogeneities lead to a wider base of the cone, our law can still be fitted to the data points. However, the accuracy of the fit improves greatly if the subsample size considered is above the percolation threshold.

This new method allows us to speed up the process of finding the REV. Instead of trying to simulate the full sample size like traditionally done for the REV convergence, a large number of small subsamples is sufficient. The computational gain obtained by reducing the size of the simulations allows to overcome the upcoming computational limitation stemming from the current increase of μCT-scan resolution testing the limits of our simulator's capacity.

CRediT authorship contribution statement

Sijmen Zwarts: Writing – review & editing, Writing – original draft, Software, Investigation, Conceptualization. **Martin Lesueur:** Writing – review & editing, Writing – original draft, Supervision, Software, Conceptualization.

Declaration of competing interest

The authors declare that they have no known competing financial interests or personal relationships that could have appeared to influence the work reported in this paper.

Data availability

Data will be made available on request.

Appendix. Computational performance

In this appendix, we approximate the evolution laws of the sample size with the memory usage and run time of our simulations based on data points from sequential runs on growing subsamples, extrapolated using a fit from the Least Square Method. The memory usage follows a linear function of the Degrees of Freedom as $a * DoFs + b$. Given the use of the Generalised Minimal Residual Method for our FEM solver, we expect and obtain a classical power law for the run time, $c * DoFs^d$. The results of the fits are shown in Fig. A.11, for which satisfying values of coefficient of determination R^2 are obtained.

For a more intuitive comparison between the sample sizes, we refer in the text to those laws with regard to cubic sample length l. Once the porosity has converged with the growing sample size, the number of degrees of freedom increases linearly with l^3. The evolution of the minimal memory requirement is therefore expressed as $a * l^3 + b$ and the simulation time $c * l^{3d}$. Despite a slightly reduced coefficient of determination, the fits continue to be adequate.

As suggested by our method, we simulate an equivalent volume of a large sample L^3 with as many subsamples as can fit within the sample. To obtain a comparison of the computational performance of our method with the traditional one that only simulates the large sample, we introduce the ratio $\eta = \frac{L}{l}$. The reduction in memory usage, determined between one subsample and the sample, can be calculated as

$$m_{rel} = \frac{a(\frac{L}{\eta})^3 + b}{aL^3 + b} = \frac{b\eta^3 + aL^3}{\eta^3(aL^3 + b)} \approx \frac{1}{\eta^3} \tag{A.1}$$

given the negligible contribution of b that corresponds to the necessary overheads of the simulator. The total speed-up obtained by using our

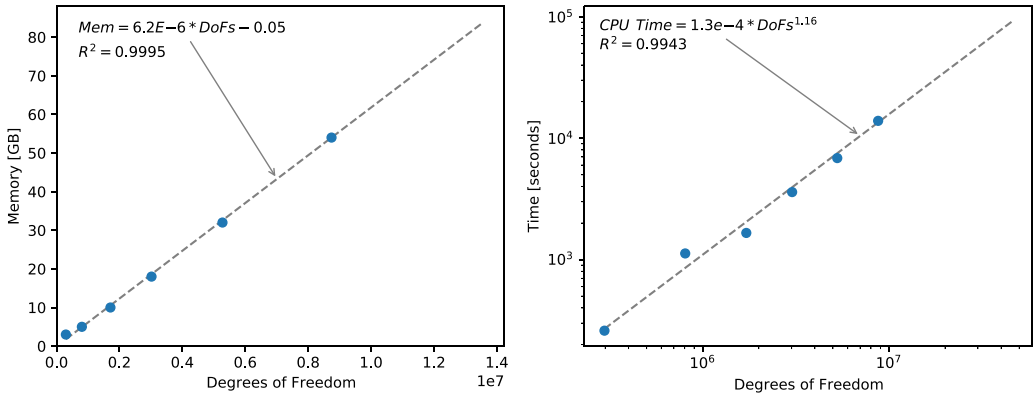

Fig. A.11. The fitted evolution laws, extrapolated to the size of the REV. The memory requirement is shown on the left side and the computational time on the right side. The blue dots are the obtained data points, the grey dashed line is the fitted function.

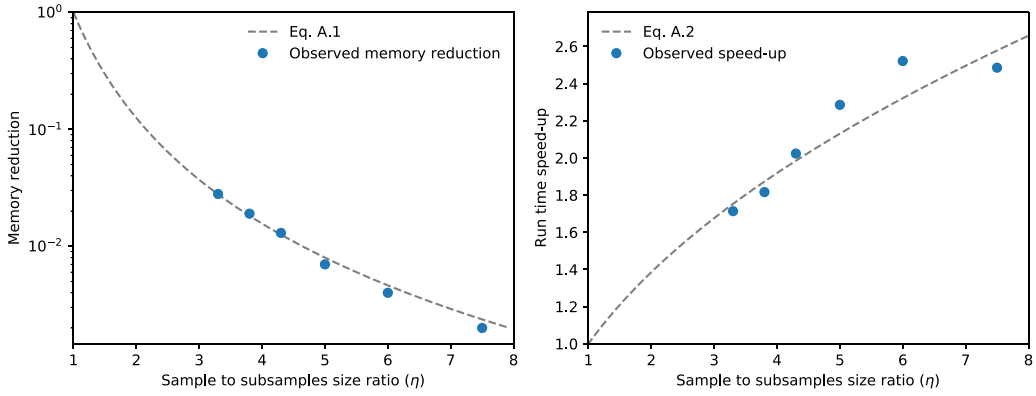

Fig. A.12. The evolution of the memory reduction on the left and the simulation speed-up time on the right, both relative to the traditional method of finding REV. The derived formulas are shown with the grey dashed line and the observed data points are shown with blue dots.

method is calculated as:

$$t_{rel} = \frac{cL^{3d}}{\eta^3 c(\frac{L}{\eta})^{3d}} = \frac{1}{\eta^{3(1-d)}} = \eta^{3(d-1)} \tag{A.2}$$

Those two formulas are plotted in Fig. A.12 against the data collected in Fig. A.11 which displays a good fit. Both memory usage and runtime of our method at the different sizes of the subsamples are compared to the traditional method for REV convergence, corresponding more specifically in this case study to the requirements for the full sample of the LV60A sandpack.

References

1. Beard DC, Weyl PK. Influence of texture on porosity and permeability of unconsolidated sand. *AAPG Bull*. 1973;57. http://dx.doi.org/10.1306/819a4272-16c5-11d7-8645000102c1865d.
2. Cox MR, Budhu M. A practical approach to grain shape quantification. *Eng Geol*. 2008;96(1–2):1–16. http://dx.doi.org/10.1016/j.enggeo.2007.05.005.
3. Torskaya T, Shabro V, Torres-Verdín C, Salazar-Tio R, Revil A. Grain shape effects on permeability, formation factor, and capillary pressure from pore-scale modeling. *Transp Porous Media*. 2014;102(1):71–90. http://dx.doi.org/10.1007/s11242-013-0262-7.
4. Thiemeyer N, Habersetzer J, Peinl M, Zulauf G, Hammer J. The application of high resolution X-ray computed tomography on naturally deformed rock salt: Multi-scale investigations of the structural inventory. *J Struct Geol*. 2015;77:92–106. http://dx.doi.org/10.1016/j.jsg.2015.05.014, URL https://www.sciencedirect.com/science/article/pii/S0191814115001133.
5. Elvin AA. Number of grains required to homogenize elastic properties of polycrystalline ice. *Mech Mater*. 1996;22(1):51–64. http://dx.doi.org/10.1016/0167-6636(95)00024-0.
6. Ren Z-Y, Zheng Q-S. Effects of grain sizes, shapes, and distribution on minimum sizes of representative volume elements of cubic polycrystals. *Mech Mater*. 2004;36(12):1217–1229. http://dx.doi.org/10.1016/j.mechmat.2003.11.002.
7. Liu C. On the minimum size of representative volume element: An experimental investigation. *Exp Mech*. 2005;45(3):238–243. http://dx.doi.org/10.1007/bf02427947.
8. Grimal Q, Raum K, Gerisch A, Laugier P. A determination of the minimum sizes of representative volume elements for the prediction of cortical bone elastic properties. *Biomech Model Mechanobiol*. 2011;10(6):925–937. http://dx.doi.org/10.1007/s10237-010-0284-9.
9. Shan Z, Gokhale AM. Representative volume element for non-uniform microstructure. *Comput Mater Sci*. 2002;24(3):361–379. http://dx.doi.org/10.1016/s0927-0256(01)00257-9.
10. Sebsadji S, Chouicha K. Determining periodic representative volumes of concrete mixtures based on the fractal analysis. *Int J Solids Struct*. 2012;49(21):2941–2950. http://dx.doi.org/10.1016/j.ijsolstr.2012.05.017.
11. Graham S, Yang N. Representative volumes of materials based on microstructural statistics. *Scr Mater*. 2003;48(3):269–274. http://dx.doi.org/10.1016/s1359-6462(02)00362-7.
12. Du X, Ostoja-Starzewski M. On the size of representative volume element for Darcy law in random media. *Proc R Soc A: Math Phys Eng Sci*. 2006;462(2074):2949–2963. http://dx.doi.org/10.1098/rspa.2006.1704.
13. Łydżba D, Różański A. Microstructure measures and the minimum size of a representative volume element: 2D numerical study. *Acta Geophys*. 2014;62(5):1060–1086. http://dx.doi.org/10.2478/s11600-014-0226-5.
14. Kanit T, Forest S, Galliet I, Mounoury V, Jeulin D. Determination of the size of the representative volume element for random composites: Statistical and numerical approach. *Int J Solids Struct*. 2003;40(13–14):3647–3679. http://dx.doi.org/10.1016/s0020-7683(03)00143-4.
15. Pelissou C, Baccou J, Monerie Y, Perales F. Determination of the size of the representative volume element for random quasi-brittle composites. *Int J Solids Struct*. 2009;46(14–15):2842–2855. http://dx.doi.org/10.1016/j.ijsolstr.2009.03.015.
16. Mirkhalaf S, Pires FA, Simoes R. Determination of the size of the representative volume element (RVE) for the simulation of heterogeneous polymers at finite strains. *Finite Elem Anal Des*. 2016;119:30–44. http://dx.doi.org/10.1016/j.finel.2016.05.004.
17. van der Meer FP. Micromechanical validation of a mesomodel for plasticity in composites. *Eur J Mech A Solids*. 2016;60:58–69. http://dx.doi.org/10.1016/j.euromechsol.2016.06.008, URL https://www.sciencedirect.com/science/article/pii/S0997753816300778.

18. Rocha I, Raijmaekers S, van der Meer F, Nijssen R, Fischer H, Sluys L. Combined experimental/numerical investigation of directional moisture diffusion in glass/epoxy composites. *Compos Sci Technol*. 2017;151:16–24. http://dx.doi.org/10.1016/j.compscitech.2017.08.002, URL https://www.sciencedirect.com/science/article/pii/S0266353817309983.
19. Rahman T, Ramandi HL, Roshan H, Iglauer S. Representative elementary volume of rock using X-Ray microcomputed tomography: A new statistical approach. *Geofluids*. 2020;2020:1–13. http://dx.doi.org/10.1155/2020/8866486.
20. Lesueur M, Guével A, Poulet T. Reconciling asymmetry observations in the permeability tensor of digital rocks with symmetry expectations. *Adv Water Resour*. 2022;170:104334. http://dx.doi.org/10.1016/j.advwatres.2022.104334.
21. Zwarts S, Lesueur M. Homogenisation method based on energy conservation and independent of boundary conditions. *Adv Water Resour*. 2024;183:104603. http://dx.doi.org/10.1016/j.advwatres.2023.104603, URL https://www.sciencedirect.com/science/article/pii/S0309170823002385.
22. Permann CJ, Gaston DR, Andrš D, et al MOOSE: Enabling massively parallel multiphysics simulation. *SoftwareX*. 2020;11:100430. http://dx.doi.org/10.1016/j.softx.2020.100430, URL http://www.sciencedirect.com/science/article/pii/S2352711019302973.
23. Peterson JW, Lindsay AD, Kong F. Overview of the incompressible Navier–Stokes simulation capabilities in the MOOSE framework. *Adv Eng Softw*. 2018;119:68–92. http://dx.doi.org/10.1016/j.advengsoft.2018.02.004, URL https://www.sciencedirect.com/science/article/pii/S0965997817310591.
24. Thovert J-F, Mourzenko VV. On the influence of boundary conditions when determining transport coefficients from digital images of heterogeneous media. *Adv Water Resour*. 2020;141:103612. http://dx.doi.org/10.1016/j.advwatres.2020.103612.
25. Altman DG, Bland JM. Standard deviations and standard errors. *BMJ*. 2005;331(7521):903. http://dx.doi.org/10.1136/bmj.331.7521.903.
26. O'neill B. Some useful moment results in sampling problems. *Amer Statist*. 2014;68(4):282–296. http://dx.doi.org/10.1080/00031305.2014.966589.
27. Lesueur M, Casadiego MC, Veveakis M, Poulet T. Modelling fluid-microstructure interaction on elasto-visco-plastic digital rocks. *Geomech Energy Environ*. 2017;12:1–13. http://dx.doi.org/10.1016/j.gete.2017.08.001.
28. Lesueur M, Rattez H, Colomés O. MicroCT scans permeability computation with an unfitted boundary method to improve coarsening accuracy. *Comput Geosci*. 2022;166:105118. http://dx.doi.org/10.1016/j.cageo.2022.105118.
29. Delft High Performance Computing Centre (DHPC). DelftBlue supercomputer (phase 1). 2022 https://www.tudelft.nl/dhpc/ark:/44463/DelftBluePhase1.
30. Imperial College Consortium on Pore-scale Imaging and Modelling. LV60A sandpack. 2014 http://dx.doi.org/10.6084/m9.figshare.1153795.v2, URL https://figshare.com/articles/dataset/LV60A_sandpack/1153795.
31. Mostaghimi P, Bijeljic B, Blunt MJ. Simulation of flow and dispersion on pore-space images. *SPE J*. 2012;17(04):1131–1141.
32. Mostaghimi P, Blunt MJ, Bijeljic B. Computations of absolute permeability on micro-CT images. *Math Geosci*. 2012;45(1):103–125. http://dx.doi.org/10.1007/s11004-012-9431-4.
33. Imperial College Consortium on Pore-scale Imaging and Modelling. S1 sandstone. 2014 http://dx.doi.org/10.6084/m9.figshare.1189274.v1, URL https://figshare.com/articles/dataset/S1_sandstone/1189274.
34. Imperial College Consortium On Pore-Scale Modelling. Ketton Limestone, URL https://imperialcollegelondon.app.box.com/v/iccpsim-ketton2015.
35. Imperial College Consortium on Pore-scale Imaging and Modelling. C2 carbonate. 2014 http://dx.doi.org/10.6084/m9.figshare.1189258.v1, URL https://figshare.com/articles/dataset/C2_carbonate/1189258.
36. Zhao B, Saxena N, Hofmann R, Pradhan C, Hows A. Enhancing resolution of micro-CT images of reservoir rocks using super resolution. *Comput Geosci*. 2023;170:105265. http://dx.doi.org/10.1016/j.cageo.2022.105265, URL https://www.sciencedirect.com/science/article/pii/S009830042200214X.
37. Omori T, Suzuki S, Michibayashi K, Okamoto A. Super-resolution of X-ray CT images of rock samples by sparse representation: Applications to the complex texture of serpentinite. *Sci Rep*. 2023;13(1). http://dx.doi.org/10.1038/s41598-023-33503-6.